Pergamon

PII: S0148-9062(96)00027-7

Int. J. Rock Mech. Min. Sci. Vol. 34, No. 1, pp. 71–84, 1997

0148-9062/97 $17.00 + 0.00

Variogram Characterization of Joint Surface Morphology and Asperity Deformation During Shearing

R. O. ROKO†
J. J. K. DAEMEN‡
D. E. MYERS§

The morphology of the joint interface is described using geostatistical parameters such as the sill, range and slope of the initial part of the variogram. The methodology is also used to identify the scale effect and to determine the appropriate cutoff length of the sample which is representative for a direct shear test. The anisotropy characteristics of the interface are described using the sill and slope of the initial portion of the variogram. The result is used to assess the flowpath for a hypothetical fluid injection test. The surface compliance of the interface subjected to shear is determined using the mean difference of the interface. The rate of deformation of the interface is represented in two-dimensions using polar coordinates. The practical implication of the rate of collapse of the loop on the stability of the translation motion is given. © 1997 *Elsevier Science Ltd. All rights reserved.*

INTRODUCTION

Interfaces in contact have a significant influence on the shear strength of a rock mass [1–5]. While this fact is widely accepted [6], uncertainty remains as to which textural features play critical roles and to what extent they are relevant. Two rocks (salt and quartz for example) with identical initial roughness characteristics do not necessarily generate the same shear resistance under identical testing conditions. The influence of the asperities decreases as the strength of the asperities decreases or when the velocity of the sliding motion is high. Whitehouse and Archard [7] point out that if the interface behaves plastically, the geometry of the asperities will have either no impact or only a marginal impact on the shear strength of the discontinuity. Therefore, the initial configuration of the interface alone is not sufficient to explain the influence of roughness on the shear strength of a rock joint. Knowledge of the deformational character of the joint interface with normal and shear loads is essential to improve our understanding of the shear resistance of rock discontinuities.

†Ore Body Engineering, 1721 E Glenn Ste. #C, P.O. Box 3573, Tucson, Arizona, U.S.A.
‡University of Reno, Mining Eng. Dept., Reno, Nevada, U.S.A.
§University of Arizona, Dept. of Mathematics, Tucson, Arizona, U.S.A.

The volumetric change which occurs during the direct shear tests conducted on rough natural joints [9] illustrates the importance of the deformation of the asperities on the transition between dilatancy and contractancy. For a given shear displacement, the greater the deformation of the asperities, the lower the dilatancy. When the deformation increases rapidly with the normal load, the shear displacement at which the contractancy begins decreases. Such a condition is bound to worsen the stability of the sliding motion. This observation has significant practical importance in slope stabilization through weight reduction where the slope is intersected by a failure plane.

During sliding motion of a confined block, any dilatancy initiates an increase in normal stress. The normal stress rises as long as the deformation of the asperities is small and the dilatancy increases. An interface having an apparent friction angle $\phi_b = \phi_r + i$ where the true contact friction angle is $\phi_r = 20°$ and the roughness angle $i = 5°$ provides greater stability than an interface having $\phi_r = 25°$ and $i = 0°$. When deformation of the asperities accompanies the shear displacement, there is a reduction in normal stress and a decrease of ϕ_b toward ϕ_r. The reduction of the normal stress will create a drop in the frictional force which may cause instability. In the case of an unconfined block, the

importance of asperity deformation will be explained through the change in potential energy. Because friction is a nonconservative force, the work done depends on the path taken. Dilatancy increases the length of the path, while an increase in asperity deformation reduces it.

The deformation of the asperities also has relevance in problems involving fluid flow. The flow regime is influenced by roughness and particularly by aperture closure and by the aperture distribution across the flowpath [6,10]. When two rough surfaces in contact are loaded, deformation of asperities results in changes in average hydraulic conductivity as well as in local true aperture. Aperture closure is due to the reduction in height of the asperities in contact and to the expansion of the contact area [11]. A reduction in aperture decreases the flow path cross-sectional area, the changes of tortuosity [12] and consequently the effect of the flow regime. Along saturated low permeability, discontinuities asperity deformation and resulting aperture changes can induce liquid pressure build-ups.

In problems such as fluid flow or discontinuity shear strength determination, the anisotropy of the interface can play a major role. When the spatial profile data are treated as if they result from a linear profile or as if they are randomly selected, it is possible to obtain two surfaces with the same roughness parameters, but with very different spatial arrangements. The spatial arrangement of the two superimposed surfaces dictates the contact zones during a translational motion and consequently the frictional resistance and the tortuosity.

This study develops a geostatistical methodology for describing discontinuity surfaces. The methodology is applied to illustrate roughness changes that take place during direct shear testing. The methodology is also used to identify the cutoff length to determine the minimum sample size to be used in the direct shear test and the flowpath during a fluid injection test. The variogram is used so that the spatial variability can be taken into account. This function allows a determination of the continuity of the height distribution, i.e. the correlation between two observations taken at two distinct points. It also allows a three-dimensional representation of the surface profile, and reveals the anisotropy of the surface structure (directional variability of the height distribution of the asperities).

The parameters considered for the characterization of the discontinuity and for the analysis of the deformation of the rock joint asperities in the case of the variogram are the sill, range and slope of the initial portion of the variogram. The sill and slope for a given discontinuity surface taken along different azimuths are plotted using polar coordinates to illustrate the directional behavior of the joint. Sequential variability of the sill and slope after each shearing is used to evaluate the rate of collapse of the directional loops, i.e. the degree of permanent deformation of the interface.

The analysis utilizes the variogram function, comprised of two curves (Fig. 1) corresponding to limiting cases: curve (I) represents the variogram of the initial

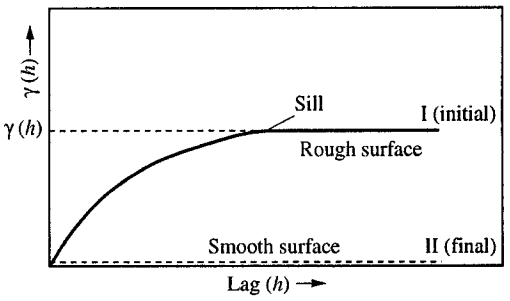

Fig. 1. Theoretical variograms representing rough (curve I) and smooth (curve II) surfaces.

configuration of the surface roughness and curve (II) represents the variogram of the surface configuration after elimination of all variation in the height of the asperities. The rate at which a transition from the initial state to the final state is accomplished is critical in describing the surface compliance. In this approach, the crucial parameters for characterization of the joint surface are the sill or maximum $\gamma(h)$ and the slope of the initial part of the variogram. The rate at which a transition occurs may be observed through the use of the loop which characterizes the surface structure (Fig. 2).

LABORATORY PROCEDURES

Topographical measurement

The topographical description of the surface discontinuity starts with measuring the elevation of the asperities at numerous discrete points. The apparatus consists of a mobile table which can slide in two perpendicular directions and a dial gage fixed above the table. Attached to the gage is a cursor which can move only vertically. A transducer with a flat edge is attached to the dial gage. Before a topographical measurement begins, a surface grid is drawn on the discontinuity surface of the sample. The grid spacing is 3.2 mm.

A systematic means of locating the nodes of the grid is devised in order to accelerate the mapping. A rigid plastic plate with markers at 3.2 mm spacings is positioned horizontally over the discontinuity surface and then lowered so that the grid can be marked on the

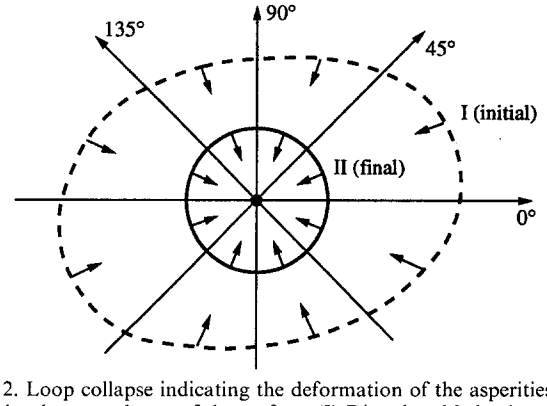

Fig. 2. Loop collapse indicating the deformation of the asperities and thereby the smoothness of the surface. (I) Directional behavior of the initial surface. (II) Directional behavior after surface deformation. The maximum variance or the sill taken at various azimuths and after each loading is used to determine the convergence.

discontinuity surface. This accelerates the grid drawing and allows precise location of the coordinates of the sheared zones after successive shearings. During the initial mapping of the surface topography, sufficient reference points are marked on the cast and on the sliding table to ensure easy and consistent repetition of the measurements.

Laboratory direct shear test

The applied normal loads are increased stepwise up to the chosen maximum. At each normal load, the sample is sheared in one direction. After each shearing, the sample is carefully returned to its initial position. The primary reason for repositioning the sample is to study the influence of multiple shearings on the same surface. Using this procedure, an evaluation can be made of the influence of successive shearings on the behavior of the same joint surface, but subjected to different loading conditions. By repositioning the two matting surfaces to their original positions, the effect of heterogeneity in the mineralogy and of differences in the initial geometry of the natural discontinuity surfaces have been taken into account. Consequently, comparisons of the interface behavior during multiple shearings could be made. No contact of the sample is allowed during the resetting. By matching at least three precast holes in the mold, the potential for surface damage during sample repositioning is averted and the resetting is completed rapidly. After each shearing, the surface topography is measured. Since the sheared zones are localized, it is not necessary to repeat the measurements over the entire sample. This approach is valid only if permanent deformation is restricted to the surface asperities. Plastic deformation of the cast due to the imposition of normal loads might create differential settlement of the sample. To prevent this, steel rods are placed underneath the sample during casting.

THE VARIOGRAM FUNCTION: SIGNIFICANCE IN SURFACE CHARACTERIZATION

Variogram parameters

In classical statistics, it is often assumed that samples taken from an unknown population are random and independent of each other; i.e. one sample does not provide any information about the next sample. This assumption implies that the position from which the sample is taken is irrelevant. Although this assumption may hold true in some circumstances, it is far from universally valid. In general, adjoining samples may reflect some degree of continuity, i.e. some correlation exists between them. When continuity among samples is apparent, the variance may be used to analyze its spatial dispersion. The variogram function describes the extent of the correlation.

The variogram $\gamma(h, \theta)$ is defined as the average of the squares of the delayed amplitude differences:

$$\gamma(h, \theta) = \tfrac{1}{2}E\{[Z(x, y) - Z\{(x, y) + h(\theta)\}]^2\} \quad (1)$$

where

$Z(x, y)$ = the height at location (x, y)
$Z\{(x, y) + h(\theta)\}$ = the height at a radial distance h in a direction θ from (x, y)
$E\{\}$ = the expectation.

The variogram function depends only on the vector h and not on the location x. This intrinsic hypothesis corresponds to the second order stationarity of the difference $[Z(x, y) - Z\{(x, y) + h(\theta)\}]$. In physical terms, it indicates that the structure of variability between $Z(x, y)$ and $Z\{(x, y) + h(\theta)\}$ is constant and thus independent of (x, y).

In the variogram shown in Fig. 1 (curve I) h represents a vector with modulus $|h|$ taken along the direction θ. With the lag equal to zero, $\gamma(h) = 0$, the variogram increases with the modulus $|h|$ until the sill is reached. If this portion of the curve characterizes the distribution of the surface asperities, it indicates that the difference in the heights at two points increases as the distance $|h|$ between the two points increases. The way in which the variogram increases for small values of $|h|$ characterizes the degree of spatial continuity of the height distribution of the asperities. For a given direction θ, as the lag h becomes large, the correlation between the variables $Z(x, y)$ and $Z\{(x, y) + h(\theta)\}$ may disappear. In this case, the variogram tends asymptotically toward a constant value. This limiting distance is called the range. It represents the area of influence beyond which sample pairs become independent and no longer correlate with one another [8]. The sill shown in Fig. 1 (curve I), when it exists, represents the transitional limit beyond which the variogram stabilizes. The difference between the sill and the value of the variogram at distance $|h|$ corresponds to the level of certainty which exists when a height is extrapolated. As the range is approached, the estimation variance increases to the level of this sill. The variogram is zero at lag zero (by definition) and the nugget is the jump at zero. The nugget incorporates the local variability, hence, it quantifies the local heterogeneity of the structure. A high nugget value relative to the sill can indicate a high degree of surface heterogeneity, i.e. the height distribution of the asperities is very irregular.

Variograms which are characterized by a sill value and a range are called transition models. They correspond to a random function which is not only intrinsic, but is also second-order stationary. In a transition phenomenon, any data value $Z(x, y)$ correlates with the value for any point within a radius (a) of (x, y). This correlation and hence the influence of one value on the other decreases as the distance between two points increases. The computation and plot of $\gamma^*(h, \theta)$ are obtained with a computer program designed to calculate the experimental variograms in any given direction within a plane using the data obtained from asperity height measurements at the coordinates (x, y) over the surface.

During a direct shear test, the motion takes place in a constant direction. Therefore, there is no interference between two adjacent points at an angle θ from the direction of sliding. Because of this physical constraint,

a two degree window is selected. A zero degree window causes a singularity problem.

Theoretical variogram models: physical significance

The most common theoretical models used to describe variograms can be divided into models without a sill and models with a sill. The models without a sill include the power model and the logarithmic model. The transition models comprise the spherical, exponential and Gaussian models. The models are.

- power model

$$\gamma(h) = \begin{cases} ah^{\lambda} + b & h > 0 \quad \text{with } \lambda \in]0, 2[\\ 0 & h = 0 \end{cases} \tag{2}$$

- logarithmic or De Wijsian model

$$\gamma(h) = a \ln(h) + b \quad \text{with} \quad \gamma(0) = 0 \tag{3}$$

- spherical model

$$\gamma(h) = \begin{cases} \frac{3}{2}\frac{h}{a} - \frac{1}{2}\frac{h^3}{a^3} & h \in [0, a] \\ 1 & h \geqslant a \end{cases} \tag{4}$$

- exponential model

$$\gamma(h) = 1 - e^{-h/a} \tag{5}$$

- Gaussian model

$$\gamma(h) = 1 - e^{-h^2/a^2} \tag{6}$$

- hole-effect model

$$\gamma(h) = \begin{cases} 1 - \sin(h)/h & h > 0 \\ 0 & h = 0 \end{cases} \tag{7}$$

where h is expressed in radians.

The initial variation of $\gamma(h)$, with increasing lag for the six models suggests that the surface is rough. The degree of roughness may be illustrated by the magnitude of the slope near the origin. The convergence toward a sill with the spherical, exponential and Gaussian models indicates a steady state roughness. A model without a sill depicts a surface with a continuous increase in roughness as the lag increases. For the hole effect, the variogram displays a non-monotonic behavior.

Anisotropy characteristics

A surface is anisotropic when certain orientations provide greater variation than others. Anisotropy analysis permits an assessment of the directional distribution of the heights of the asperities. When the function $\gamma(h, \theta)$ depends only on the modulus $|h|$ the phenomenon is said to be isotropic.

To quantitatively identify the anisotropic behavior, the maximum value of the variogram function is determined in different orientations. If the loop formed by the maxima can be approximated by a circle of radius $\gamma(h)$, i.e. $\gamma(h, \theta) = \gamma(h)$ for all directions θ, the variable being investigated is said to be isotropic. If the loop can be approximated by an ellipse, it is considered a geometric anisotropy. If the graph does not conform to either of the two preceding forms, it is considered to display zonal anisotropy [8].

RELATION BETWEEN SURFACE MORPHOLOGY AND VARIOGRAM PARAMETERS

To illustrate the physical implications of the variograms, some basic hypothetical profiles are considered. Five surface profiles are generated using parametric sine equations: $Z = a_1 \sin(\omega x)$, where a_1 is the amplitude of oscillation and ω the wavelength. By varying the amplitude and wavelength, five surface profiles are generated, as shown in Figs 3(a) and 4(a)–(d). Each figure describes an undulating smooth surface.

Figures 3(a), and 4(a) and (b) possess the same amplitude, but different wavelengths (2.5, 1.0 and 5.7 mm, respectively). In Fig. 4(a) and (b), the amplitude of oscillation is 0.1 with two different wavelengths (1.0 and 5.7 mm). The objective of the variogram analysis is to establish the correlation between the roughness characteristics of the surface profile and the variogram parameters, such as the slope of the initial portion of the variogram, the sill and the range.

To identify the anisotropy of the surface, the sample variogram is computed along five directions (0°, 30°, 45°, 60° and 90°). The analysis is confined to quadrant I because the studied profiles have axes of symmetry. Along the azimuth 0° there is no variation of the surface profile, hence $\gamma(h) = 0$. Along the remaining four azimuths [Fig. 3(b)–(e)], in the initial portion of the variogram, $\gamma(h)$ increases as h increases. Depending on the direction of the azimuth, different physical characteristics are captured. As the frequency increases, the slope for the initial part increases. The higher the frequency, the greater the slope angle is for a given direction and for two different surfaces, the higher $\gamma(h)$ for a given lag, the rougher the surface. For a given lag, $\gamma(h)$ increases as the azimuth increases, which is compatible with the geometry of the surface. The variogram can also be used to represent the peaks of the surface variation. The variograms clearly identify the periodicity displayed by the surface profile. When the amplitude of the oscillation decreases [Fig. 4(c) and (d)], the slope of the initial portion decreases. Therefore, the smoothing of a surface following shearing can be analyzed through the use of the variogram.

ANALYSIS AND DISCUSSIONS OF THE RESULTS

The variogram analysis of the spatial distribution of asperities is conducted on a quartz porphyry, a diorite and a pebble sample. The analysis focuses on the experimental and theoretical variograms. Three parameters used to describe the surface roughness are the sill, slope and range of the variogram. It is assumed that the sampling length is small enough so that the result represents the surface topography. The relationship between the roughness and the three variables is

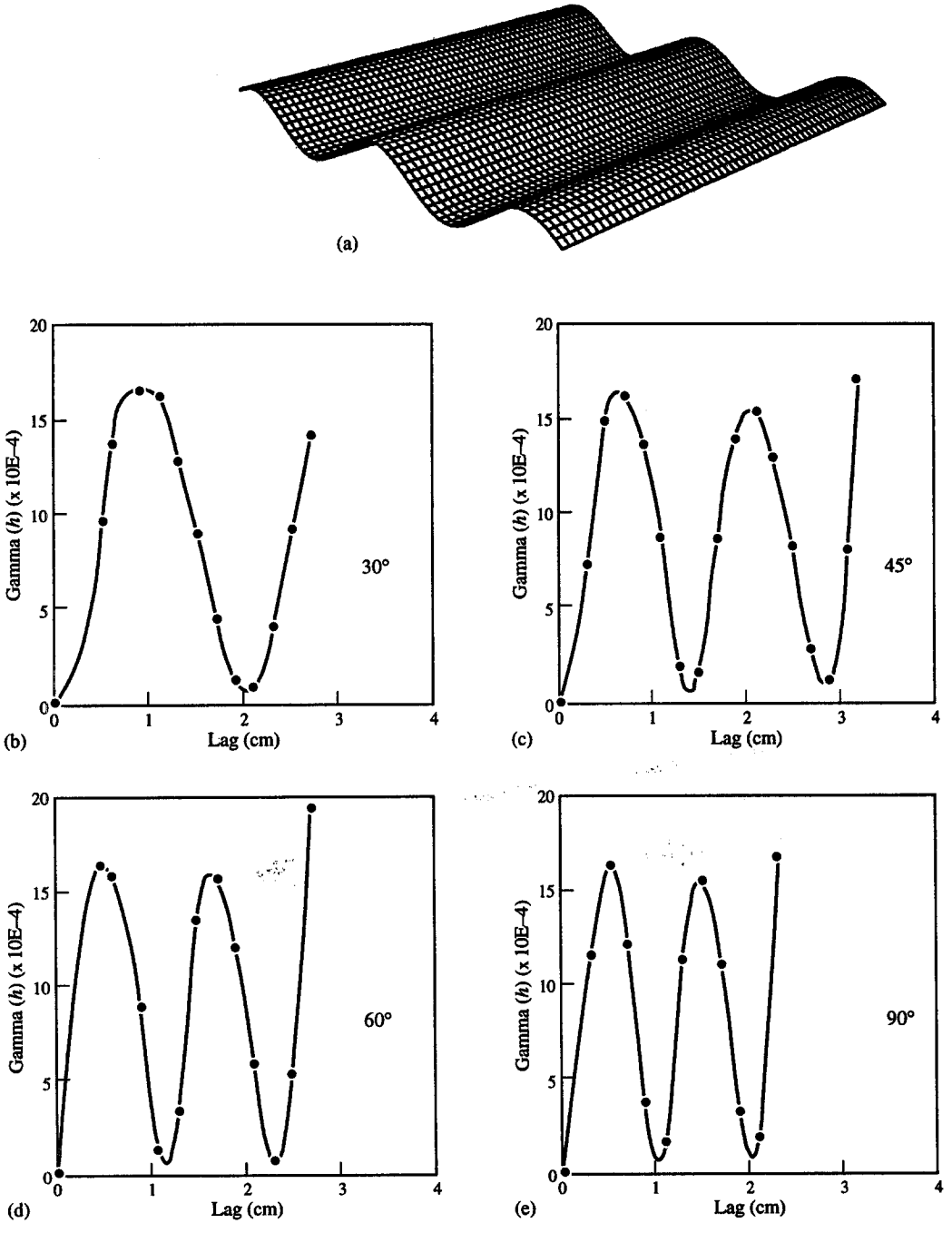

Fig. 3. Undulating smooth surface and corresponding variograms taken along the azimuths 30°, 45°, 60° and 90°.

demonstrated. The experimental variograms are indicated by dotted lines and the theoretical variograms by solid lines (Figs 5–7).

Experimental variograms

Figure 5(a) and (b) depicts the joint surface topography of the quartz porphyry sample. The experimental variograms shown in Fig. 5(c)–(f) describe the variogram of the initial surface morphology of the sample. The variograms are computed along four azimuths (0°, 45°, 135° and 90°). The directions along which the variograms are computed are indicated on the block diagram and on the surface contour plot.

All four variograms show zero nugget, indicating that there is no sudden change in the roughness of the discontinuity at small lags. This observation was predictable since the sampling is done at regular and small intervals. The rate of increase of $\gamma^*(h)$ for small values of h suggests a relatively high continuity of the interface structure. The distribution of $\gamma^*(h)$ [Fig. 5(a)–(f)] for small h shows a slight non-linearity. This behavior may be explained by a lack of homogeneity in roughness as the lag increases. The slope of the initial portion of the curves indicates that the roughness increases with the lag up to 45.0 mm. If such behavior persists over a large distance, it would produce a scale effect as described by Bandis *et al.* [4], thereby no distinct correlation lengths will exist. The correlation lengths or ranges of the quartz porphyry sample vary between 40.0 and 50.0 mm.

The experimental variograms also present some differences. Beyond the range in Fig. 5(c), the variogram is quite homogeneous. The range in this instance may be used as the cutoff length to determine the minimum sample size to be used in the direct shear test. A constant $\gamma^*(h)$ beyond the range indicates that for a lag greater than 45.0 mm, there is homogeneity in the surface roughness. Beyond 80.0 mm lag, a local drift occurs, which is identifiable on the block diagram and on the contour plot. The physical structure responsible for the local drift is the waviness which is highlighted on the contour plot.

Beyond the sill in Fig. 5(d), the variogram is non-homogeneous. This behavior is evident on the contour plot [Fig. 5(b)]. This variogram describes the so-called hole effect. The physical attribute of this hole

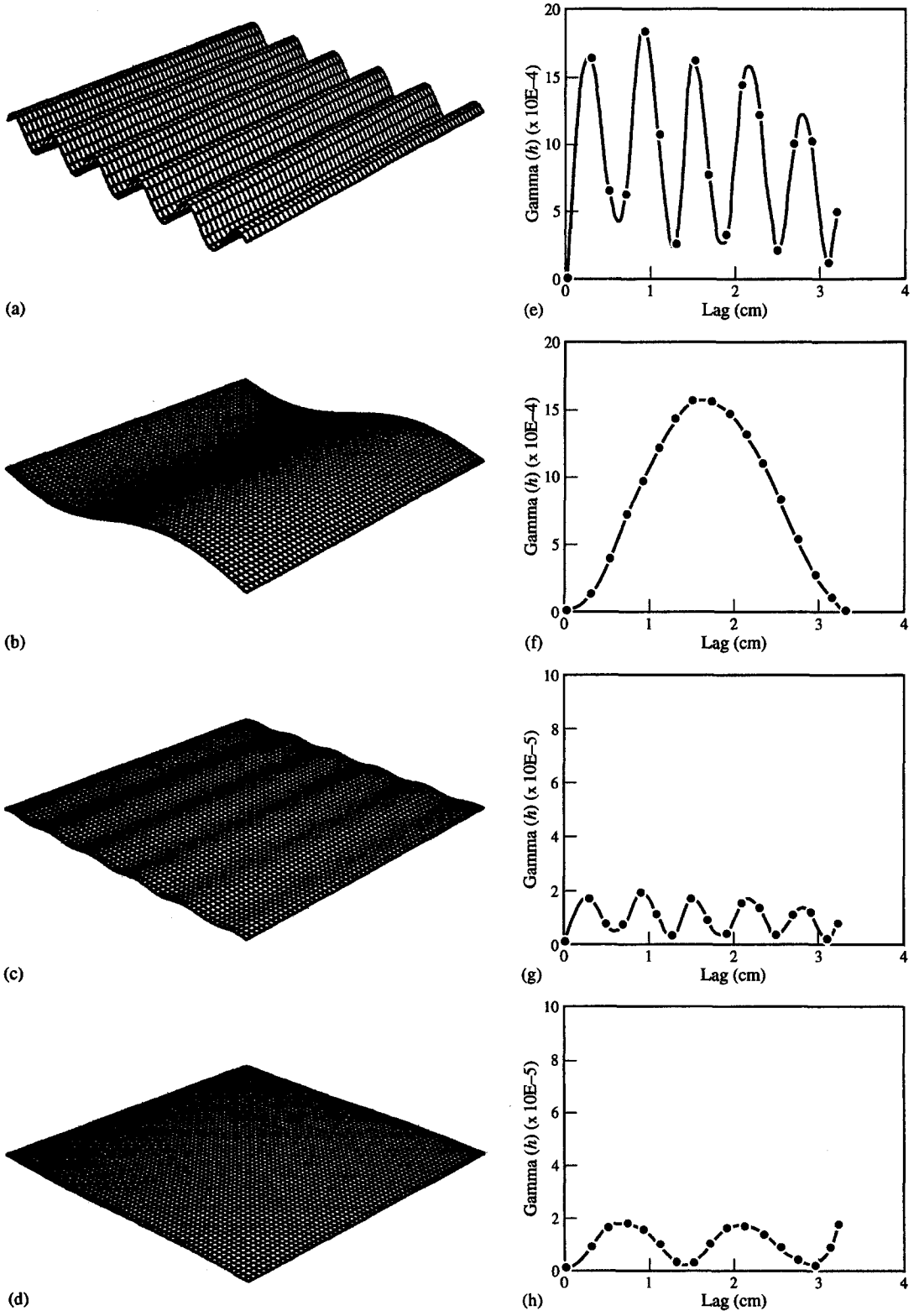

Fig. 4. Relation between surface morphology and variogram characteristics. The variograms are computed along the azimuth 45°.

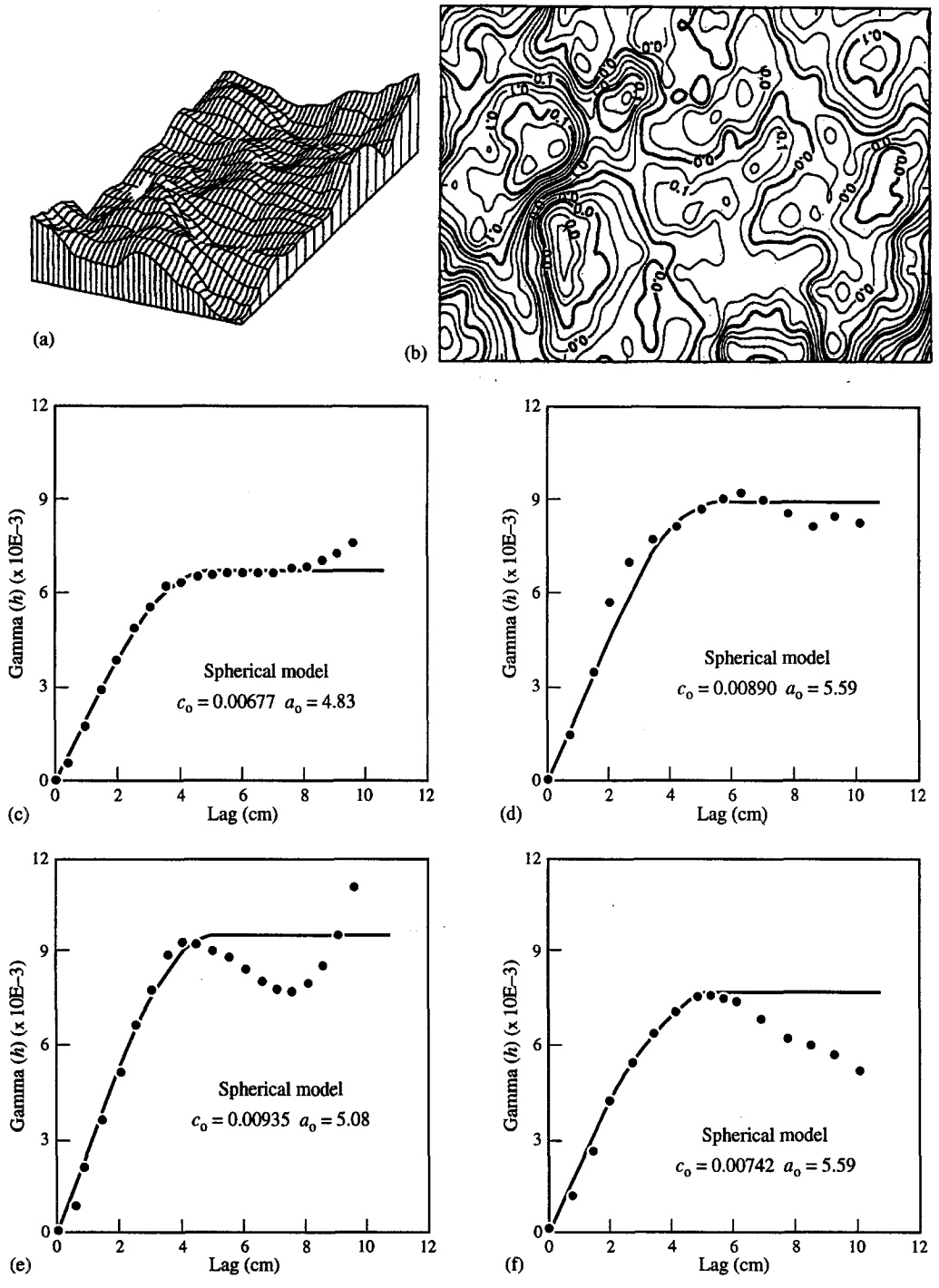

Fig. 5. Experimental and theoretical variograms for the initial surface configuration of the quartz porphyry sample taken along different azimuths. (c) 0°, (d) 45°, (e) 90°, (f) 135°. —— Theoretical, ····· Experimental.

effect is that there exists a succession of small scale undulations along the direction of the azimuth 45°. Figure 5(c) and (f) shows pronounced drifts. $\gamma^*(h)$ decreases steeply at the sill level and then increases rapidly at a 71.0 mm lag in the case of the variogram computed along the 90° direction. While a cut-off length may be justified along 0° and 45° due to the homogeneity in the variogram behavior beyond the sill, it is not acceptable along 90° and 135° azimuth because of the size effect.

Figure 6 shows the variograms which describe the initial roughness of the pebble breccia sample. The experimental variogram in Fig. 6(c) is stepwise parabolic with no distinct correlation length, i.e. $\gamma^*(h)$ increases as the lag increases. This trend is observed despite the fact that sufficient precautions were taken to properly level the discontinuity surface prior to any topographical measurement. This behavior illustrates the size effect along 0° direction. The roughness of the surface is characterized by a strong waviness along the azimuth 0° [see Fig. 6(a)]. Besides the difference in the magnitude of the sill and the range, the same non-homogeneity described in Fig. 6(a) can be observed in Fig. 6(d)–(f).

Figure 7 shows the variograms which depict the initial roughness of the diorite sample. Contrary to the

behavior observed with the quartz porphyry and the pebble breccia, there is no distinct sill or range for this sample size. $\gamma^*(h)$ continues to increase even at 100 mm lag. It is evident that the stabilization of the variogram is not yet reached. These variograms illustrate quite well the size effect.

Theoretical variograms

To determine the variogram parameters such as the sill and the range, theoretical models which best fit the experimental variograms are applied to the experimental model. The formulation of a perfect theoretical model to describe the experimental variogram is extremely difficult and there is no systematic means of determining the theoretical equation. Therefore, good judgment is needed to recognize a suitable model and then to maintain consistency when several surfaces must be compared. a_0 and c_0 designate, respectively, the range and sill of the spherical model.

The behavior of the experimental variogram for the quartz porphyry is best described using a spherical model (Fig. 5). A spherical variogram describes a linear variation between $\gamma^*(h)$ and the lag near the origin. It is followed by a yield zone which is depicted by a gradual reduction in the slope of the curve and then a plateau where the slope is zero. In practical terms, the behavior

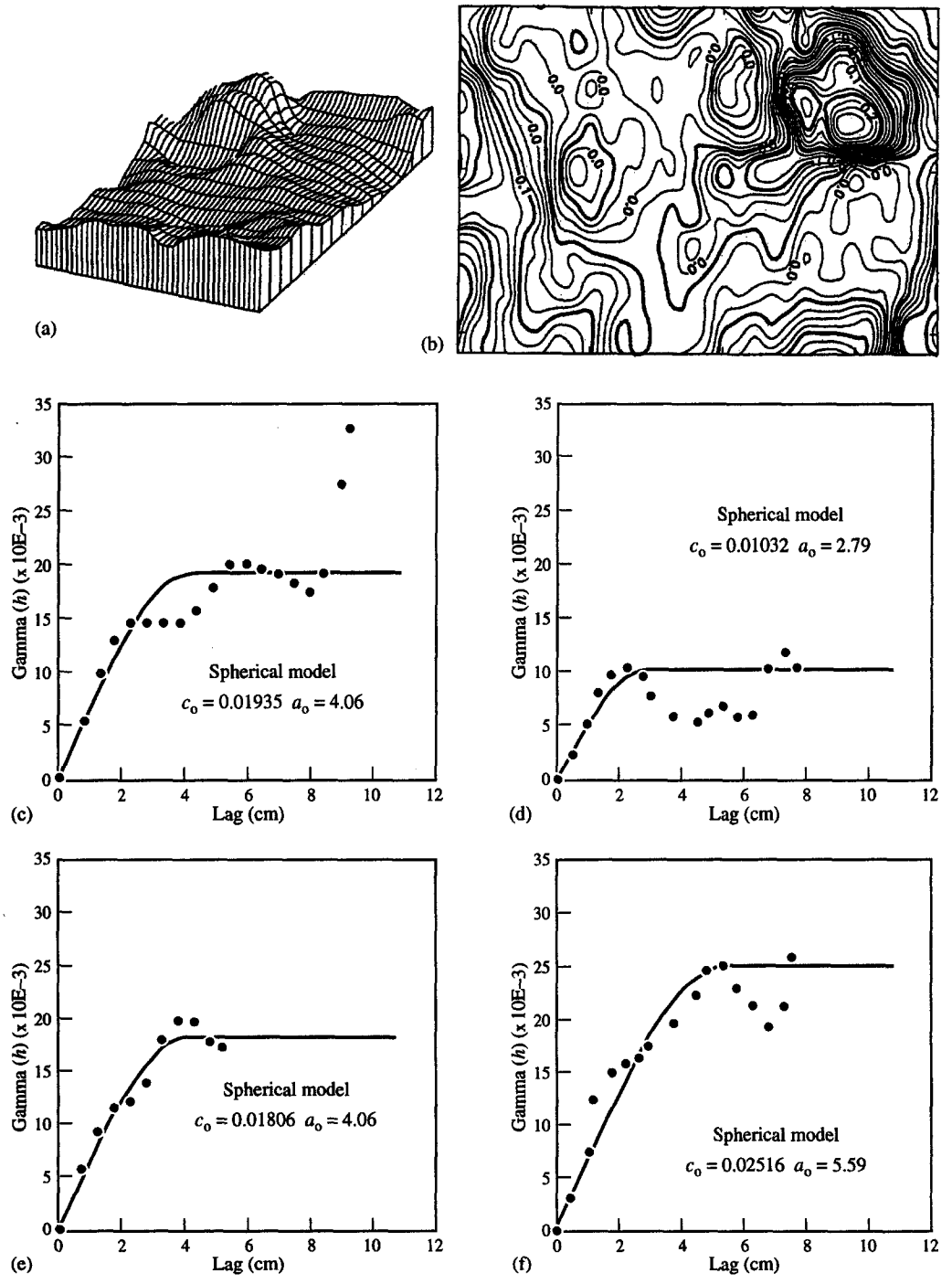

Fig. 6. Experimental and theoretical variograms for the initial surface configuration of the pebble breccia sample taken along different azimuths. (c) 0°, (d) 45°, (e) 90°, (f) 135°. —— Theoretical, ····· Experimental.

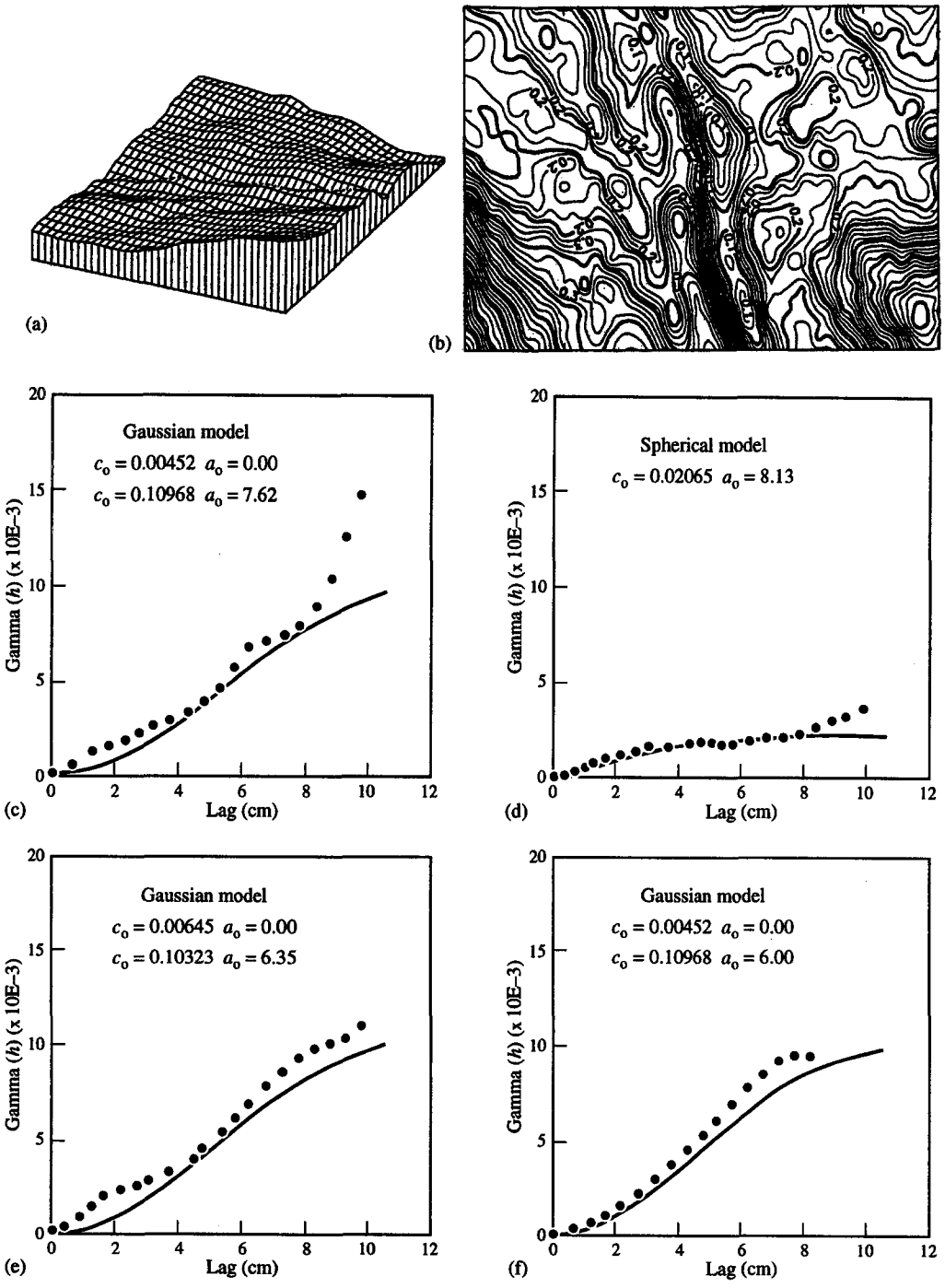

Fig. 7. Experimental and theoretical variograms for the initial surface configuration of the dionite sample taken along different azimuths. (c) 0°, (d) 45°, (e) 90°, (f) 135°. —— Theoretical, ····· Experimental.

of the spherical model implies that there is a linear increase in roughness for a small lag until a constant variance occurs, i.e. a finite limit at which the behavior becomes homogeneous. There is no influence of the size effect beyond the range. There are some deviations between the experimental and theoretical variograms. The experimental variogram near the origin is not exactly linear. Beyond the range, Fig. 5(d) and (e) shows a very large deviation between the experimental and theoretical variograms. The experimental $\gamma(h)$ is not constant for increasing lag. The overall fitting approximates the spatial distribution of the asperities.

Despite the apparent differences between the four experimental curves depicted in Fig. 6, the theoretical model which best describes the experimental variograms is the spherical model. Figure 7 depicts the theoretical variograms derived from the experimental variograms along four azimuths for the diorite sample. There are two distinct theoretical models which describe the diorite surface depending on the selected direction. The Gaussian model is more appropriate along the azimuths 0°, 90° and 135°, while the spherical model fits quite well the measured data taken along the 45° azimuth. A Gaussian structure is characterized by an increase of the slope of the variogram with an increase in lag up to a peak, followed by an asymptotic decay to zero. In

physical terms, the roughness increases with the lag and stabilizes over a long range. When a surface roughness is characterized by a Gaussian structure, it displays a size effect over a long range.

Directional behavior of the variograms

The directional behavior of the roughness described is analyzed by considering the overall variograms along four orientations (0°, 45°, 90° and 135°) and the corresponding parameters such as the sill, range of the correlated length and slope near the origin. Figure 5(c)–(f) shows the experimental and theoretical variograms which describe the initial configuration of the quartz porphyry sample. The non-linear behavior of the initial portion of the variogram is similar in all four directions. The degree of variation of $\gamma^*(h)$ with h within the correlated length is, however, somewhat different. Beyond the range, the variograms are dissimilar in all four directions. Each variogram describes a specific directional surface structure. Along the azimuth 0°, the structure is homogeneous once the range is exceeded except for the late increase of $\gamma^*(h)$ around the 76.0 mm lag. Along the 45° azimuth, on the other hand, the surface is characterized by continuous undulation. This characterizes regular low amplitude waviness of the physical sample. The amplitude and period of oscillation of the waviness are more pronounced along the 90° and 135° azimuths.

Figure 6(c)–(f) shows the directional variograms which describe the initial configuration of the pebble breccia sample. There is a strong similarity in the roughness structure along all four azimuths. The variation of $\gamma^*(h)$ with h is, however, quite different.

Figure 7(c)–(f) describes the directional roughness of the diorite sample. Along the 0°, 45°, 90° and 135° azimuths $\gamma^*(h)$ increases continuously with the lag. There is no distinct sill value when the experimental variogram is considered. Along the 90° azimuth a sill is reached at the 76.0 mm lag. The magnitude of $\gamma^*(h)$ along the 45° azimuth compared to that in the remaining three directions implies a smooth profile along that azimuth.

For each variogram, the sill, range of the correlated length and slope near the origin are determined. The magnitude of each parameter is then plotted on a polar coordinate to show their variation with orientation. Because of the existence of a symmetry, the second half of each plot is systematically extrapolated (180°, −45°, −135° and −90°). Figure 8 depicts the directional behavior of the sill of the variogram prior to shearing for the quartz porphyry, pebble breccia and diorite samples. When the variogram exhibits a transition structure, a finite plateau is reached after a finite range. The sill which is the maximum variance of the height of the interface asperities is then used to describe the anisotropic character of the surface. In Fig. 8(a) along the 0° azimuth, the magnitude of the sill is 0.0067 cm^2. The magnitude of the sill increases as one moves counterclockwise until it reaches 0.009 cm^2 along the 90° azimuth. It then decreases to 0.007 cm^2 along 135° azimuth. This directional variation of the sill indicates a geometrical anisotropy which is elliptical. The major and minor axes of this ellipse are along 70° and −20°, respectively. The sill is minimum along the azimuth 135° for the pebble breccia and along 45° for the diorite. The diorite and pebble breccia samples [Fig. 8(b) and (c)] reveal zonal anisotropy. The magnitude of the sill needs to be considered with respect to the grid size. The variogram is influenced by the grid size because of the filtering effect due to the grid spacing. If the sill is determined at the cutoff point (i.e. at the optimal grid size), it can represent the roughness characteristic of the surface.

The slope of the initial part of the variogram describes the degree of roughness with increasing lag and it may vary with direction if some anisotropy exists. If the surface is smooth planar, the slope tends toward zero, since there is no variation in elevation between any two adjacent points. When the surface is rough, the slope depends on the degree of roughness. The greater the roughness, the steeper the slope. The smaller the slope is the smoother the surface in that specific direction. For the diorite sample [Fig. 9(c)] the slope is minimum along the direction 45°, while it is maximum along 135°.

To illustrate the physical attributes of the range, consider two surfaces described by a spherical model having the same sill but different slopes. The smaller the slope is, the larger the range. The range must be analyzed in conjunction with the magnitude of the sill. A large range with a low sill indicates a smooth planar interface, while a large range with a large sill indicates a smooth undulating structure.

Table 1. Variogram parameters obtained from the spherical model prior to and after shearing for the quartz porphyry top sample

Azimuth (degree)	Load (kN)	Sill (cm^2) × 10^{-3}	Range (cm)	Slope (degree)
0°	0	6.77	4.83	48.0
	13.50	6.26	5.33	43.0
	31.45	5.81	6.35	35.0
45°	0	8.90	5.59	52.5
	13.50	8.26	5.84	48.0
	31.45	7.68	6.86	41.0
90°	0	9.35	5.08	55.5
	13.50	8.90	5.21	53.0
	31.45	8.13	6.10	46.0
135°	0	7.42	5.59	45.5
	13.50	6.77	6.35	40.0
	31.45	6.26	6.86	35.5

ANALYSIS OF SURFACE GEOMETRY CHANGES INDUCED BY SHEARING

To analyze the deformation behavior of the discontinuity following shearing, the change in slope of the variogram near the origin and the sill are considered. Figure 10 shows the experimental variograms after shearings at 4.30, 13.50, 22.50 and 31.40 kN normal force for the quartz porphyry sample and along the azimuths 0°, 45°, 90° and 135°. With an increasing normal load, the magnitude of $\gamma(h)$ for any given lag decreases. It is also evident that the sill and slope

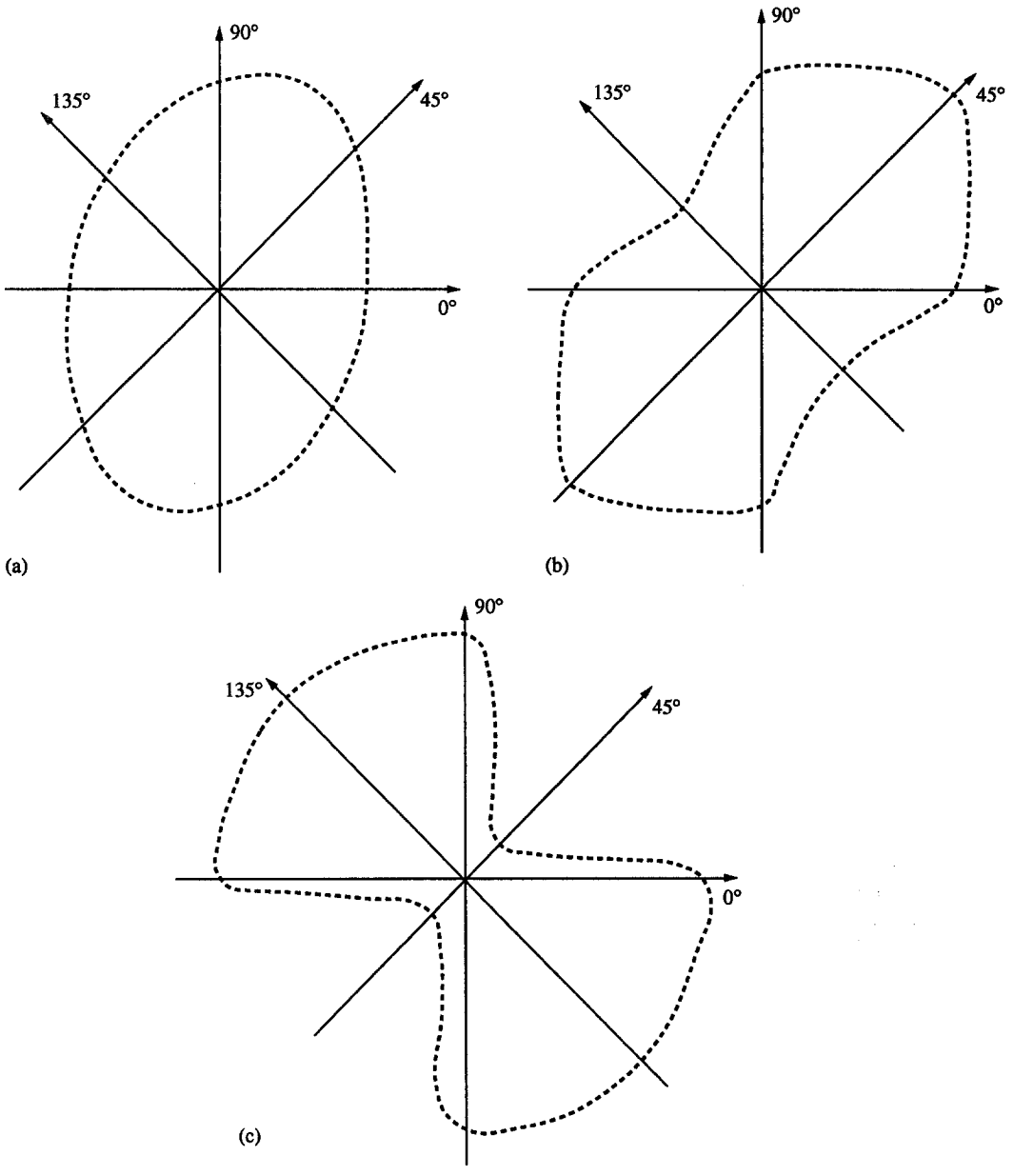

Fig. 8. Directional behavior of the variogram sill prior to shearing. (a) Quartz porphyry, (b) pebble breccia, (c) diorite. (a) Geometrical anisotropy, (b) and (c) zonal anisotropy.

decrease with increasing normal load. A smoothing effect is produced by shearing at increasing normal loads. Figure 11 shows the theoretical variograms after successive shearings of the quartz porphyry sample. The variation of the range, sill and slope are given in Fig. 11. While the sill and slope decrease with normal load, the range increases which signifies a smoothing of the interface.

The sill is plotted in polar coordinates to describe the anisotropy. Figure 12 presents the variation of the $\gamma(h, \theta)_{max}$ at three different normal loads. The curves were obtained along the 0°, 45°, 90° and 135° azimuths, and they are interpolated between the azimuths. Curve (I) corresponds to the initial surface, i.e. prior to any shearing. The inner curves correspond to the surface configuration following direct shearing at 13.50 kN and 31.40 kN normal forces, respectively. Each curve is an ellipse with a major axis along the 25° azimuth. The directional behavior of the variogram function is characterized by geometric anisotropy. The directional anisotropy is the same at 0 kN, 13.50 kN and 31.40 kN. Despite the shearing, the original anisotropy remains, which indicates a high resistance to deformation when the interface is subjected to shear. The low rate of decrease indicates that the asperities are persistent. An asperity is persistent if either the entire asperity or a portion of it still exists after shearing. The degree of persistence of the asperities after shearing depends on their hardness, shape, and imposed normal and shear loads, as well as on the loading conditions. Permanent deformation of the asperities occurs only if the stresses exceed the shear strength of the asperities. If the strength is not exceeded, dilatancy occurs for motion to proceed therefore the asperities in contact will persist. Asperities will also persist if no contact has taken place at some discrete zones during shearing.

MECHANICAL IMPLICATIONS OF THE DEFORMATION OF THE ASPERITIES

The average difference can be used to analyze the surface compliance. The experimental variogram function for discrete data is:

$$\gamma^*(h) = \frac{1}{2N}\sum_{i=1}^{N}[Z(x_i) - Z(x_i + h)]^2.$$

The average difference is:

$$H_j = \frac{1}{N}\sum_{i=1}^{N}[Z(x_i) - Z(x_i + h)]$$

where j stands for each stage of normal load. The average closure or relative normal displacement after shearing is: $\Delta H = (H_0 - H_j)_{\text{top}} - (H_0 - H_j)_{\text{bottom}}$. H_0 and H_j correspond to the average asperities height prior and after shearing, respectively. The normal compliance of the surface is expressed as:

$$\frac{1}{K_n} = \frac{\Delta H}{\Delta \sigma_n}$$

where ΔH is the relative displacement and $\Delta\sigma_n$ the change in the normal stresses.

SUMMARY AND CONCLUSIONS

The variogram function is used to characterize rock surface roughness and to study change in rock interface roughness resulting from shearing. The analysis is divided into two parts: the experimental variogram and the theoretical variogram. The variation of $\gamma(h)$ with increasing lag is first used to describe the character of the surface roughness. Theoretical curve fitting is then applied for each experimental variogram. The sill and slope for each theoretical variogram are determined, and their change as a result of shearing is analyzed to evaluate the permanent interface deformation.

The directional distribution of the asperities and its variation after successive shearings are presented. To analyze the directional behavior, the sill and slope are determined along four azimuths. Loops which describe the anisotropy characteristics are drawn in polar coordinates using the sill and initial slope of the variogram.

This analysis shows that roughness characteristics can be identified using the variogram function. The lower the slope, the smoother the surface. For a given slope, the higher the sill is the larger the range and the higher the spatial variability. Near the origin, all the variograms reveal a stationary Gaussian structure. They also show zero nugget, which indicates that there is no sudden change in roughness of the discontinuity.

The anisotropy analysis shows that the sill and slope vary with direction. A pseudo-periodicity behavior, or an increase or decrease of $\gamma(h)$ beyond the range is an indication of the size effect. This result corroborates Barton's tilt test approach for roughness characterization. It is evident from this analysis that not all discontinuities will show evidence of size effect. Two types of anisotropy are observed: the quartz porphyry sample exemplifies geometric anisotropy, while the diorite and pebble breccia samples depict zonal anisotropy. The marginal rate of the loop collapse observed for the quartz porphyry implies that the discontinuity interface has a relatively high hardness.

When the anisotropy analysis is conducted, the direction of a low sill represents the global flowpath. The tortuosity will control the microvariations of the flow

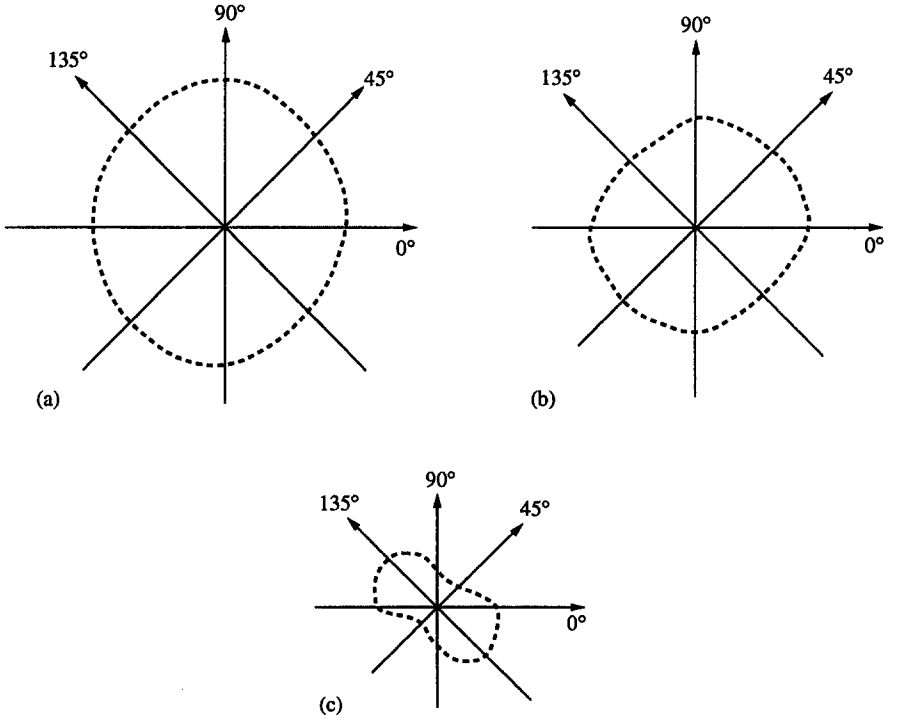

Fig. 9. Directional behavior of the variogram slope prior to shearing. (a) Quartz porphyry, (b) pebble breccia, (c) diorite.

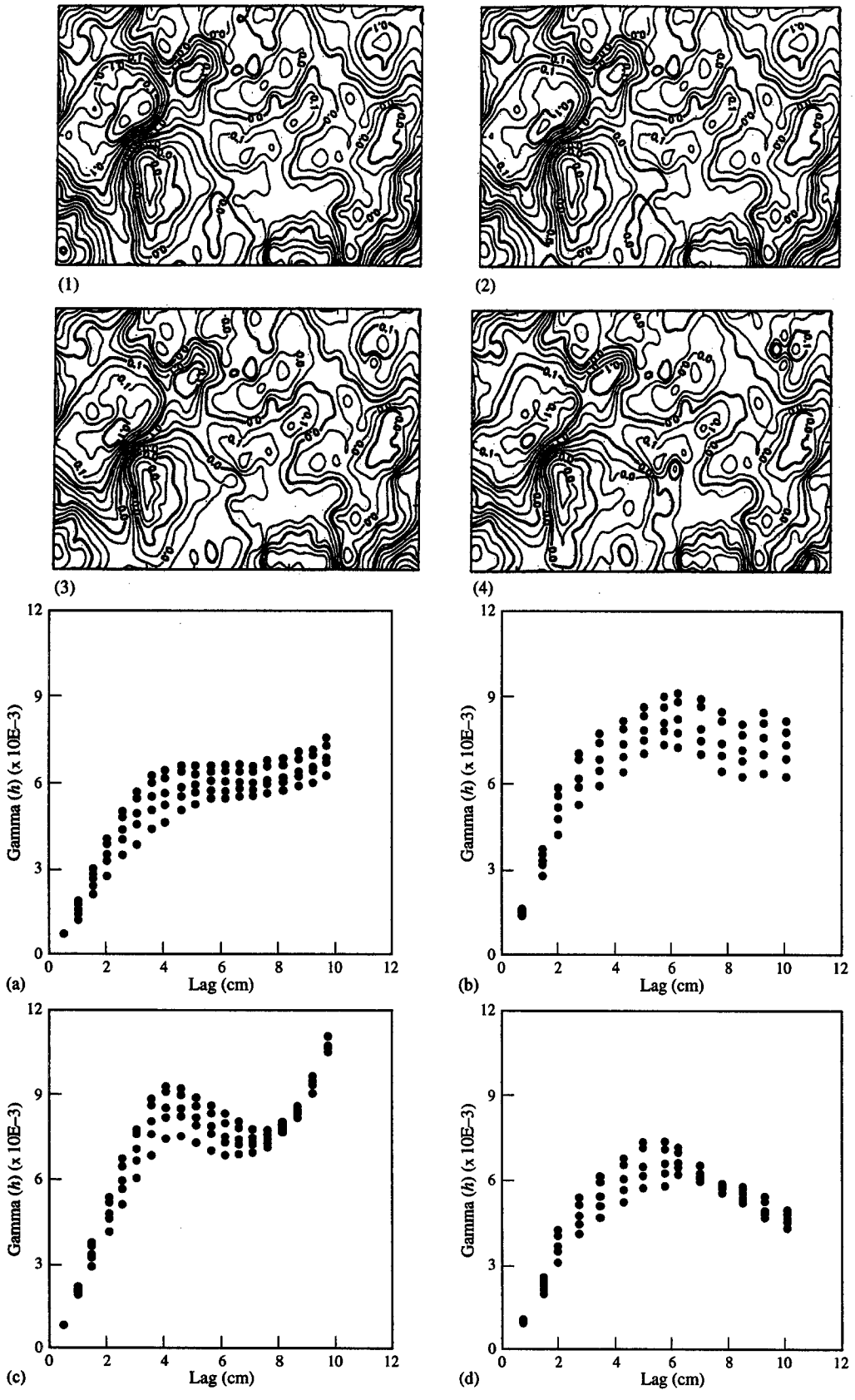

Fig. 10. Experimental variograms of the quartz porphyry sample after successive shearings at the following normal loads. (1) 4.30 kN, (2) 13.50 kN, (3) 22.50 kN, (4) 31.45 kN. (a) 0°, (b) 45°, (c) 90° and (d) 135°.

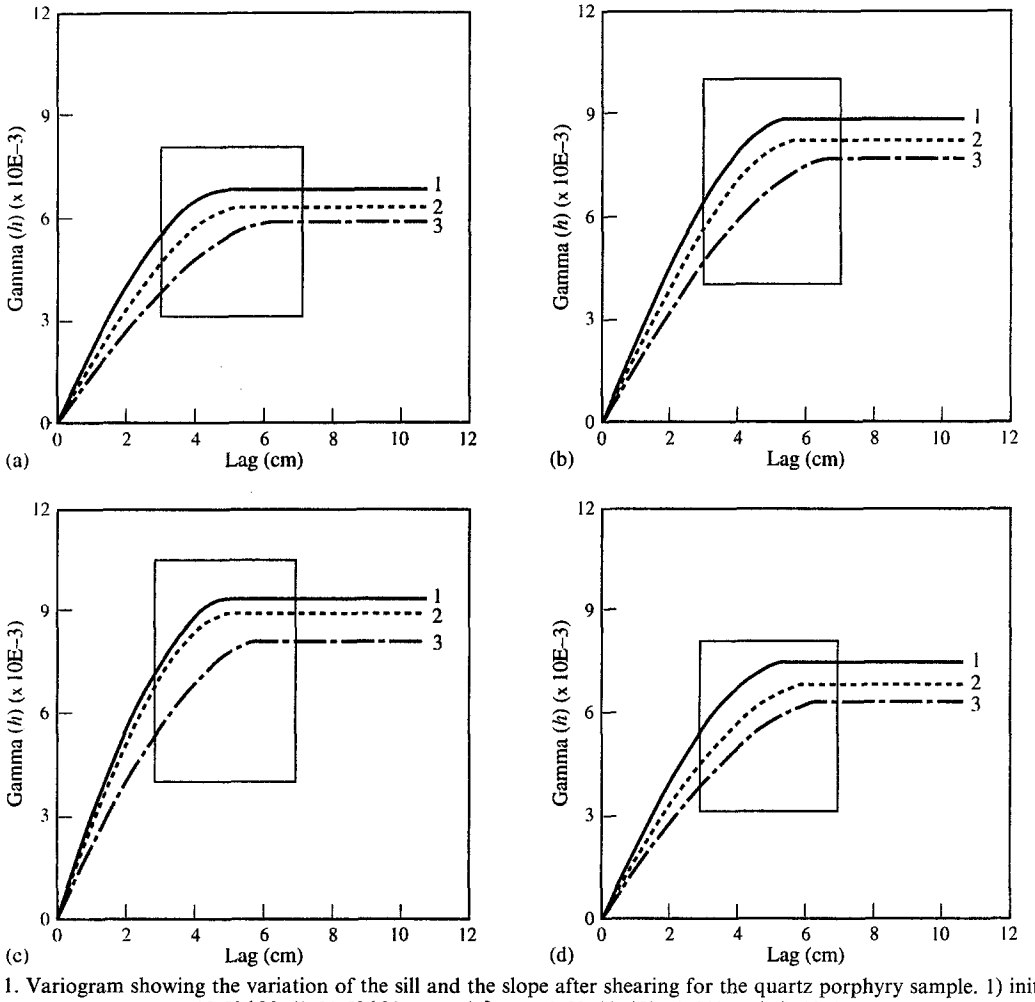

Fig. 11. Variogram showing the variation of the sill and the slope after shearing for the quartz porphyry sample. 1) initial, 2) 13.50 kN, 3) 31.50 kN normal force. a) 0°, b) 45°, c) 90° and d) 135°.

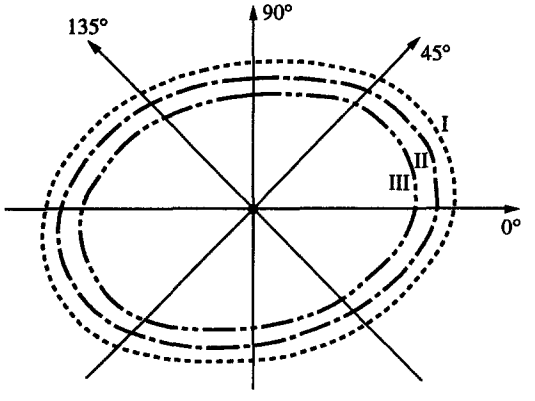

Fig. 12. Directional variation of the variogram sill for the quartz porphyry sample. Curve I is $\gamma(h, \theta)_{max}$ for the initial surface with no normal force. Curve II is $\gamma(h, \theta)_{max}$ for the surface after shearing at a 13.50 kN normal force. Curve III is $\gamma(h, \theta_{max})$ after shearing at a 31.50 kN normal force. The surface appears to be anisotropic and remains so after successive shearings.

direction. The direction of high sill will presumably provide the higher resistance.

Accepted for publication 13 June 1996.

REFERENCES

1. Byerlee J. D. Frictional characteristics of granite under high confining pressure. *J. Geophys. Res.* **72,** 3639 (1967).
2. Byerlee J. D. Brittle-ductile transition in rocks. *J. Geophys. Res.* **73,** 4741–4750 (1968).
3. Fecker E. and Rengers N. Measurement of large scale roughness of rock planes by means of profilograph and geological compass. *Rock Fractures Proc. Int. Symp. Rock Mech.* (1971).
4. Bandis S., Lumsden A. C. and Barton N. R. Experimental studies of scale effects on the shear behavior of rock joints. *Int. J. Rock Mech. Min. Sci. & Geomech. Abstr.* **18,** 1–21 (1981).
5. Barton N. The shear strength of rock and rock joints. *Int. J. Rock Mech. Min. Sci. & Geomech. Abstr.* **13,** 255–279 (1976).
6. Thomas T. R. *Rough Surfaces.* Longman Group (1982).
7. Whitehouse D. J. and Archard J. F. The properties of random surfaces of significance in their contacts. *Proc. Roy. Soc. Lond.* **A316,** 97–121 (1970).
8. Journel A. G. and Huijbregts Ch. J. *Mining Geostatistics.* Academic Press (1978).
9. Roko R. O. Influence of roughness on strength and deformation behavior of rock discontinuities. Ph.D. Dissertation, University of Arizona, Tucson Arizona (1989).
10. Schaffer A. and Daemen J. J. K. Experimental assessment of the sealing effectiveness of rock fracture grouting. NUREG/CR-4541, prepared for Division of Engineering Safety Office of Nuclear Regulatory Research U.S. Nuclear Regulatory Commission, by the Department of Mining and Geological Engineering, University of Arizona, Tucson (1987).
11. Hopkins D. L., Cook N. G. W. and Myer L. R. Fracture stiffness and aperture as a function of applied stress and contact geometry. 673-680. *Proceedings of the 28th U.S. Rock Mechanics Symposium,* Tucson, Az. (Edited by I. W. Farmer *et al.*), A.A. Balkema, Rotherdam (1987).
12. Tsang Y. W. The effect of tortuosity on fluid flow through a single fracture. *Water Resources Res.* **20,** 1209–1215 (1984).